

# Local Convolution Enhanced Global Fourier Neural Operator For Multiscale Dynamic Spaces Prediction

Xuanle Zhao<sup>1,2,\*</sup>; Yue Sun<sup>1,\*</sup>; Tielin Zhang<sup>1,2,†</sup>; Bo Xu<sup>1,2</sup>

<sup>1</sup>Institute of Automation, Chinese Academy of Sciences

<sup>2</sup>School of Artificial Intelligence, University of Chinese Academy of Sciences

zhaoxuanle2022, yue.sun, tielin.zhang, boxu@ia.ac.cn

## Abstract

Neural operators extend the capabilities of traditional neural networks by allowing them to handle mappings between function spaces for the purpose of solving partial differential equations (PDEs). One of the most notable methods is the Fourier Neural Operator (FNO), which is inspired by Green’s function method and approximate operator kernel directly in the frequency domain. In this work, we focus on predicting multiscale dynamic spaces, which is equivalent to solving multiscale PDEs. Multiscale PDEs are characterized by rapid coefficient changes and solution space oscillations, which are crucial for modeling atmospheric convection and ocean circulation. To solve this problem, models should have the ability to capture rapid changes and process them at various scales. However, the FNO only approximates kernels in the low-frequency domain, which is insufficient when solving multiscale PDEs. To address this challenge, we propose a novel hierarchical neural operator that integrates improved Fourier layers with attention mechanisms, aiming to capture all details and handle them at various scales. These mechanisms complement each other in the frequency domain and encourage the model to solve multiscale problems. We perform experiments on dynamic spaces governed by forward and reverse problems of multiscale elliptic equations, Navier-Stokes equations and some other physical scenarios, and reach superior performance in existing PDE benchmarks, especially equations characterized by rapid coefficient variations.

## 1. Introduction

Conventional research in the deep learning field is predominantly driven by neural networks designed to learn relationships between input and output pairs that lie in finite-dimensional spaces. These advancements have led to no-

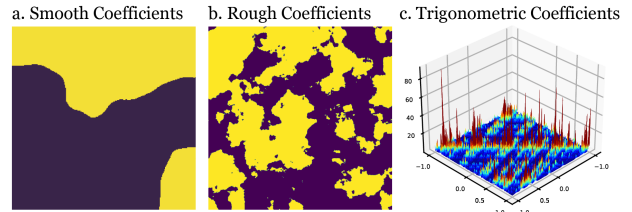


Figure 1. The difference between conventional and multiscale PDE input coefficients, where (a) denotes conventional PDE coefficients, (b) and (c) denote the multiscale PDE coefficients. In (a), the input coefficients are smooth, resulting in a smooth solution space. However, in (b) and (c), the coefficients become rough and oscillating, making the solution space difficult to solve.

table breakthroughs in numerous domains, including computer vision [4, 20], natural language processing [7, 50], reinforcement learning [17, 49], and signal processing [8, 13]. Recently, how to utilize deep learning models to solve scientific or natural problems has garnered the attention of many researchers [18].

Partial differential equations (PDEs) are utilized in scientific researches to describe a wide variety of physical, chemical, and biological phenomena [42, 48]. From turbulent flows to atmospheric circulation and material stress analysis, numerous real-world phenomena are fundamentally governed by the underlying PDEs. Therefore, solving PDEs is an important component of addressing natural science problems.

Traditional numerical methods such as the finite element method (FEM) and the finite difference method (FDM) present challenges in terms of incorporating noisy data, generating complex meshes, solving high-dimensional problems, and handling inverse problems. Fortunately, leveraging the expressivity of neural networks, many innovative works have been proposed to effectively overcome the limitations of numerical methods in solving PDEs and remarkable success has been achieved [2, 19, 28, 29]. Examples of such methods include physics-informed neural networks (PINN) [25] and Galerkin transformers (GT) [3],

\*These authors contributed equally.

†Corresponding author

which are specifically designed neural networks for PDE simulation by estimating the mapping between inputs and output pairs. In addition, methods such as the deep operator network (DeepONet) [32] and the Fourier Neural Operator (FNO) [26, 27] attempt to learn an operator between input and output function spaces. Besides solving PDEs, these methods have also proven to be effective in dealing with issues related to complex dynamics such as climate change and natural disasters [11, 37].

We consider dynamic spaces governed by multiscale PDEs in this work, which are widely used in physics, engineering, and related disciplines for analyzing complex practical problems such as reservoir modeling, air and ocean circulation, and high-frequency scattering [38]. As multiscale PDEs are characterized by rapidly changing coefficients and oscillations in the solution space, it is crucial to capture information across a variety of scales and frequency ranges to effectively address them. Nevertheless, when applied to solving PDEs, FNO and related methods tend to prioritize learning low-frequency components [1, 26, 30]. Therefore, how to capture high-frequency features and combine them with low-frequency features of the FNO is crucial for solving multiscale PDEs.

In this paper, we presented a novel method that attempts to integrate low-frequency and high-frequency features at different scales. Since the convolution kernel is locally computed, high-frequency local details can be captured efficiently. Therefore, inspired by DCNO [1], we adopt the Fourier kernel with the convolutional-residual layer, which aims to improve the ability to capture high-frequency information. Also, we attempt to add large kernel attention (LKA) after the Fourier layer to capture high-frequency components and integrate information from different channels. The LKA is composed of depth-wise convolution and channel attention and absorbs the advantages of them. To capture information at various scales, we propose a hierarchical structure model that learns convolutional-residual Fourier layers and attentions at different scales. Our main contributions can be summarized as follows:

- We propose a novel method that approximates the mapping between input and output function spaces at different scales in hierarchical structures and enhances the Fourier neural operator to combine with convolution and large kernel attention to balance the high-frequency and low-frequency features.
- Our method outperforms previous methods in dynamic spaces governed by existing PDE benchmarks, such as Navier-Stokes equations and Darcy equations, especially multiscale elliptic equations characterized by rapidly changing coefficients and solution variations.
- Our method shows effectiveness and robustness in solving inverse problems of multiscale PDEs with noisy input data.

## 2. Background and related works

We briefly cover the background and related works in this section.

### 2.1. Neural PDE solver

A number of excellent works have been done previously on solving PDEs using neural networks [18, 31]. PINN [25] employs neural networks to parameterize the solution and combine the equations and explicit constraints of PDEs (e.g., initial and boundary conditions) with the supervised loss as the optimization target. GT [3] utilizes attention-based operator learners to solve PDEs and designs Fourier-type and Galerkin-type attention with linear complexity. Neural operators leverage the concept that the operator denotes the mapping between input and output function spaces. DeepONet [32] leverages the universal approximation theorem to derive a branch-trunk structure to form the operator. Some other methods incorporate trained neural networks into conventional numerical solvers, to minimize numerical errors when dealing with coarse grids [5, 33]. Our approach is built on the concept of FNO [26, 27] and shows promising results in solving multiscale PDEs.

### 2.2. Multiscale PDEs

Multiscale PDEs have many applications and are crucial to atmospheric convection and ocean circulation, including the modeling of subsurface flow pressures [9, 24], the deformation of linearly elastic materials [34, 41], and the electric potential of conductive materials [43]. Multiscale elliptic partial differential equations are classic examples of multiscale PDEs. For smooth coefficients, solving the elliptic PDEs is a conventional problem and could be easily solved by FNO and relevant methods. However, when the coefficient becomes rapidly changing, values of the solution spaces present oscillations and high contrast ratios [1]. Another example is turbulent flow, which can be modeled using the Navier-Stokes equation. This equation describes fluid flow and exhibits turbulent behavior at high Reynolds numbers. In turbulent flow, unsteady vortices interact with each other, resulting in complex dynamics. Equations and more details about multiscale PDEs are presented in Sec. 4. To solve these kinds of multiscale PDEs, models should have the ability to extract global and local information.

### 2.3. Fourier Neural Operator

The Fourier neural operator (FNO) [26, 27] draws inspiration from the conventional Green’s function method and directly optimizes the kernel within the Fourier frequency domain by utilizing the Fast Fourier Transform (FFT), which has been proved to be an efficient way of reducing computational cost and global convolution. A notable advancement is that the operator kernel is directly trained in the frequency

domain, the network is theoretically independent of the resolution of the training data. Thus, FNO [26, 27] can deal with super-resolution problems and can be trained on multiple PDEs with the help of a consistent underlying architecture.

The FNO has established the cornerstone of operator learning, and subsequently, there have been several works inspired by the FNO. Geo-FNO [27] deforms the irregular grid into a latent space with a uniform grid to solve the limitation of FFT which could only be applied to rectangular domains. F-FNO [44] learns the kernel weights in a factorized way with separable spectral layers. G-FNO [21] utilizes the symmetry groups in the Fourier kernel to learn equivalent representations and improve accuracy even under imperfect symmetries.

Furthermore, networks inspired by FNO have been verified in various domains, including computer vision and time series forecasting [35, 36]. AFNO [12] leverages kernel in the Fourier domain as a token mixer within the transformer, aiming at reducing computational complexity and enhancing performance in segmentation tasks. FEDformer [51] harnesses sparse basis elements in the Fourier frequency domain to create a frequency-enhanced Transformer. Meanwhile, GFNet [40] employs the element-wise multiplication of learnable global filters with features in the frequency domain to improve the performance in classification and transfer learning tasks.

However, FNO ignores high-frequency components by default to learn a smooth representation of the input space, which results in poor performance when solving partial differential equations with rapidly changing coefficients [30]. To address this limitation, we propose the addition of the convolutional-residual layer and large kernel attention [15] to the structure. More details are introduced in Sec. 3.

## 2.4. Visual Attention methods

The attention mechanism can be regarded as a process of adaptive selection based on input features. It has yielded advantages in numerous visual tasks, including image classification [45], object detection [6, 22], and semantic segmentation [10, 47]. In computer vision, the attention mechanism can be divided into three main categories: channel attention, spatial attention, and temporal attention. Recent research in visual attention aims to integrate the strengths of various attention mechanisms to create more holistic attention [14, 23].

## 3. Methods

In this section, we introduce our proposed method in detail. First, we formulate operator learning problems and illustrate FNO only learning the low-frequency domain. Then, we introduce the architecture of our method.

### 3.1. Problem Formulation

For a problem governed by a partial differential equation (PDE), the observed samples are  $(a_i, u_i)_{i=1}^N$ . Assuming the coordinates in a bounded open set  $\mathcal{D} \subset \mathbb{R}^d$ , both the input and output can be expressed as functions with respect to these coordinates. These functions belong to the Banach spaces  $\mathcal{X} = \mathcal{X}(\mathcal{D}; \mathbb{R}^{d_a})$  and  $\mathcal{Y} = \mathcal{Y}(\mathcal{D}; \mathbb{R}^{d_u})$  respectively. Here,  $\mathbb{R}^{d_a}$  and  $\mathbb{R}^{d_u}$  denotes the range of input and output functions.  $\mathcal{D}$  consists of a finite set of grid points within a rectangular area in  $\mathbb{R}^2$ . The function values are represented by position  $x \in \mathcal{D}$ , which could be denoted as  $a(x)$  and  $u(x)$ . The overall solving process could be viewed as using a neural network  $f_\theta$  to approximate the mapping  $\mathcal{X} \rightarrow \mathcal{Y}$  to learn the operator, which  $\theta$  denotes the network parameter.

The Fourier neural operator is a powerful and efficient architecture for modeling partial differential equations that learns operators for mapping input and output function spaces. This algorithm is inspired by Green’s function method by learning the kernel integral operator defined below.

**Definition 3.1.** Define the kernel integral operator mapping by

$$[\mathcal{K}(\phi)a](x) = \int k_\phi(x, y)a(y)dy, \quad \forall x \in \mathcal{D}, \quad (1)$$

where Green’s function  $k_\phi$  is parameterized by neural networks with  $\phi$ .

In this context, the function  $k_\phi$  serves as a kernel function that is learned from data. FNO assumes that Green’s function is periodic and only dependent on the relative distance, which means that  $k_\phi(x, y) = k_\phi(x - y)$ . Then the operation in Eq. 1 could be regarded as convolution and efficiently implemented as element-wise multiplication in the frequency domain by using the convolution theorem

$$\begin{aligned} [\mathcal{K}(\phi)a](x) &= \int k_\phi(x - y)a(y)dy \\ &= \mathcal{F}^{-1}(\mathcal{F}(k_\phi) \cdot \mathcal{F}(a))(x) \\ &= \mathcal{F}^{-1}(R_\phi \cdot \mathcal{F}(a))(x), \end{aligned} \quad (2)$$

where  $\mathcal{F}$  and  $\mathcal{F}^{-1}$  are the Fourier transform and the inverse Fourier transform respectively. Instead of learning the kernel  $k_\phi$ , FNO directly learns the kernel  $R_\phi$  in the Fourier domain.

It is important to note that although the integral operator itself is linear, the neural operator has the ability to learn non-linear operators by using non-linear activation functions. Thus, the Fourier layer can be formally expressed as

$$\hat{u}(x) := \sigma(Wa(x) + \mathcal{F}^{-1}(R_\phi \cdot \mathcal{F}(a))(x)), \quad \forall x \in \mathcal{D},$$

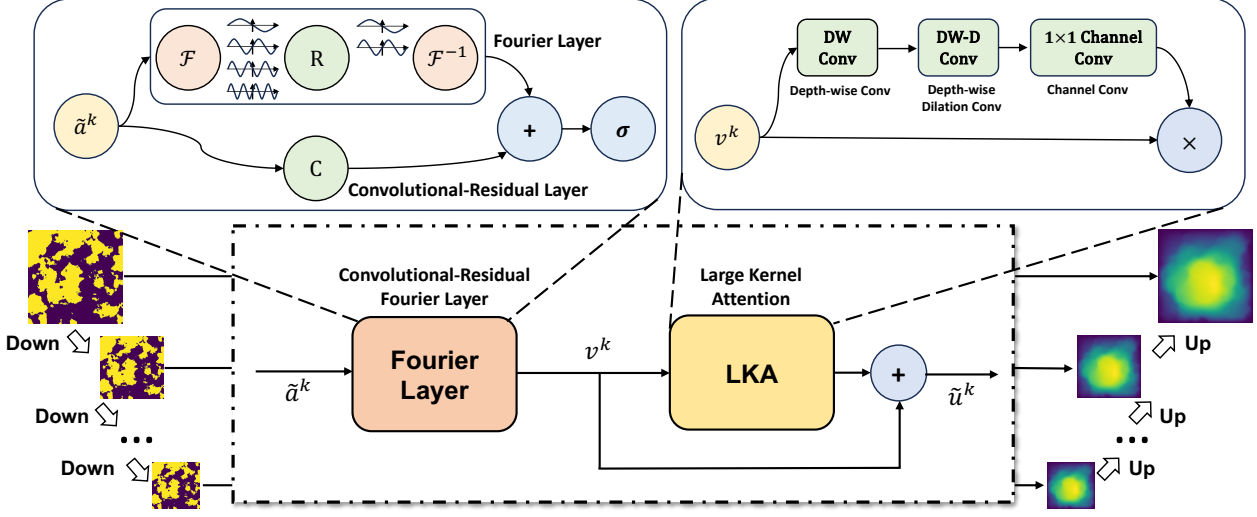


Figure 2. Network architecture. The solving process is applied to each scale with convolutional-residual Fourier layer and large kernel attention successively.

where  $\sigma$  denotes the non-linear activation function,  $W$  and  $R_\phi$  are the fully-connected layer and trainable operator kernel respectively.

Nevertheless, the next statement will show that high-frequency features are not well represented in FNO and related methods, which poses a challenge in dealing with multiscale PDEs. During the Fourier transformation process of the FNO, only the low-frequency components ( $\omega \leq T_\omega$ ) are reserved for multiplication, and high-frequency components ( $\omega > T_\omega$ ) are ignored by default. The size of the kernel is the same as the size of the low-frequency components that are reserved. Thus the elementwise multiplication process could be expressed as

$$(R_\phi \cdot \mathcal{F}(a))(\omega) = \begin{cases} (R_\phi \cdot \mathcal{F}(a))(\omega), & \omega \leq T_\omega, \\ 0, & \omega > T_\omega. \end{cases}$$

Therefore, after inverse Fourier transformation,

$$\mathcal{F}^{-1}(R_\phi \cdot \mathcal{F}(a))(x) = \sum_{\omega \leq T_\omega} (R_\phi \cdot \mathcal{F}(a))(\omega) e^{i\omega x},$$

only the low-frequency components are represented. It should be noted that for the sake of notational convenience, we only use the one-dimensional case for illustration. Additionally, previous works [30] also inform that FNO and GT have shown their tendency to prioritize learning low-frequency components before high frequencies when applied to multiscale PDEs.

However, in order to solve multiscale PDEs, it is essential to obtain information about different frequencies of the input functions. Motivated by the need to handle PDEs at different scales, this paper introduces a new hierarchical architecture neural operator.

### 3.2. Model architecture

We propose a hierarchical structure Fourier neural operator which combined with convolutional-residual layers and large kernel attention to learn the function mapping at various resolutions.

**Convolutional-Residual Fourier layers:** Inspired by DCNO [1], we propose the convolution-residual Fourier layers which are composed of two main components. In the first component, the input feature is transformed into the frequency domain by the Fast Fourier Transform and directly learning of an element-wise weight in the frequency domain. We follow the setting of FNO, only reserving lower-frequency components and training the kernel weights on them. This setting aims to learn a smooth mapping to avoid jagged curves in solution spaces. However, this setting may ignore some details about the solution space, especially in solving multiscale PDEs. Since convolution utilizes a much smaller kernel size than the Fourier transform allowing the kernel to capture locally detailed information, we replaced the fully connected residual layers with a convolution layer. This approach pertains to the high-frequency components that are overlooked by the Fourier layer. In addition, the output of the two parts is combined using the GELU activation function. To prevent confusion, we simplify the coordinates  $x$  using  $\tilde{a}^k$  and  $v^k$  as the input and output of the convolutional-residual Fourier layer at the  $k$ -th scale respectively. Thus, the Fourier layers could be modulated as:

$$v^k = \sigma(\text{Conv}(\tilde{a}^k) + \mathcal{F}^{-1}(R_\phi \cdot \mathcal{F}(\tilde{a}^k))), \quad (3)$$

where  $\sigma$  denotes the GELU activation,  $R_\phi$  represents the kernel weights in the Fourier domain that should be trained. Although the convolutional residual layers help to capture



some high-frequency features, relying solely on this component is not enough to capture all detailed information. Therefore, an alternative mechanism needs to be employed to enhance the extraction and combination of diverse frequency information. We additionally leverage the use of LKA to help extract and integrate information.

**Large kernel attention:** The attention mechanism can be seen as a dynamic selection process, where it chooses important features while automatically disregarding irrelevant parts of the input features. The attention mechanism is suitable for learning dependence among pixels in the computer vision field [10, 47]. Generally, the grid data in this work is similar to pixel images. However, previous channel and spatial attention mechanisms process the feature globally to learn the attention maps, which do not emphasize important high-frequency edge information. In this way, we apply LKA [15] that is inspired by the depth-wise convolution to capture the long-range relationship. LKA decomposes the attention into three components: a spatial local depth-wise convolution, a spatial long-range depth-wise dilation convolution, and a channel convolution with  $1 \times 1$  kernel. To prevent confusion, we use  $\tilde{u}^k$  as the output of the LKA. The LKA module could be written as

$$\begin{aligned} \mathcal{A} &= \text{Conv}_{1 \times 1}(\text{Conv}_{\text{DW-D}}(\text{Conv}_{\text{DW}}(v^k))), \\ \tilde{u}^k &= \mathcal{A} \otimes v^k, \end{aligned} \quad (4)$$

where  $v$  is the output of Convolution-Residual Fourier layers,  $\text{Conv}_{\text{DW}}$ ,  $\text{Conv}_{\text{DW-D}}$  and  $\text{Conv}_{1 \times 1}$  denote the depth-wise convolution, depth-wise dilation convolution, and channel convolution respectively.  $\otimes$  denotes the element-wise product. The value in attention map  $\mathcal{A}$  signifies the relevance of each feature. LKA integrates attention mechanisms with large receptive fields and convolution with the ability to extract local context information while maintaining linear complexity. Moreover, LKA performs both in spatial and channel domains to learn the attention map.

**Hierarchical architecture:** We attempt to train our model hierarchically, with various scales as inputs. As in multiscale PDEs, various scales and regions represent different physical laws [25]. The final prediction output is obtained by successively upsampling the outputs in different scales from coarse to fine. Specifically, for the  $k$ -scale,  $\tilde{u}^k$  is concatenated with the interpolation-upsampled  $\tilde{u}^{k+1}$  and further projected with a linear layer. Detailed information about downsampling and unsampling is presented in the Appendix. As the weight matrix is directly parameterized in the Fourier domain, we follow the FNO [26] to limit the Fourier series by terminating it at a predefined number of modes. In simple terms, we employ different truncation values at different hierarchical layers to ensure that our model can learn diverse information at different scales. However, large truncation modes would cause computing resources to increase hugely. In order to balance the computation cost

and performance, we set the truncation mode to decrease with the feature scale, as we reckon that large-scale features need more Fourier modes to represent.

### 3.3. Evaluation metrics

Previous works [1, 30] proposed H1 loss to solve multiscale PDEs which calculates the loss in the Fourier domain. However, we only use the normalized mean squared error (L2) as the loss function and evaluation metrics, which is defined as

$$\text{N-MSE} = \frac{1}{B} \sum_{i=1}^B \frac{\|\hat{u}_i - u_i\|_2}{\|u_i\|_2}, \quad (5)$$

where  $\|\cdot\|_2$  is the 2-norm,  $B$  is the batch size,  $u$  and  $\hat{u}$  are the network output prediction and ground truth respectively.

## 4. Experiments

We evaluate our proposed model on various benchmarks, including dynamic spaces governed by multiscale PDEs, Navier-Stokes Equations, and some other scenarios.

**Benchmarks.** We evaluate our method on various PDEs-governed prediction benchmarks, including multi-scale elliptic equations with various resolutions, Navier-Stokes equations with different viscosity coefficients, and other physics scenarios governed by PDEs. Also, we experiment on the inverse problem of multiscale elliptic equations with noise added to input data.

**Baselines.** We compare our method with recent and advanced methods. FNO [26], U-NO [39], and F-FNO [44] are FNO-relevant methods that use Fourier transformation to learn the operators directly in the frequency domain. WMT [16] learns the projection of the kernel onto fixed multiwavelet polynomial bases. GT [3] modify the self-attention to Fourier-type and Galerkin-type attentions with linear complexities to solve the PDEs. HANO [30] utilizes hierarchical attention to solve multiscale PDEs. LSM [46] solves the PDEs in the latent spectrum domain by decomposing latent features into basic operators.

### 4.1. Multiscale Elliptic Equations

The multiscale elliptic equation is given by a second-order linear elliptic equation,

$$\begin{cases} -\nabla \cdot (a(x)\nabla u(x)) = f(x), & x \in D, \\ u(x) = 0, & x \in \partial D, \end{cases} \quad (6)$$

with rough coefficients and Dirichlet boundary. Our model aims to approximate an operator, which maps the input coefficient function to the corresponding output solution space. In contrast to previous works, the coefficient functions show a significant degree of smoothness, leading

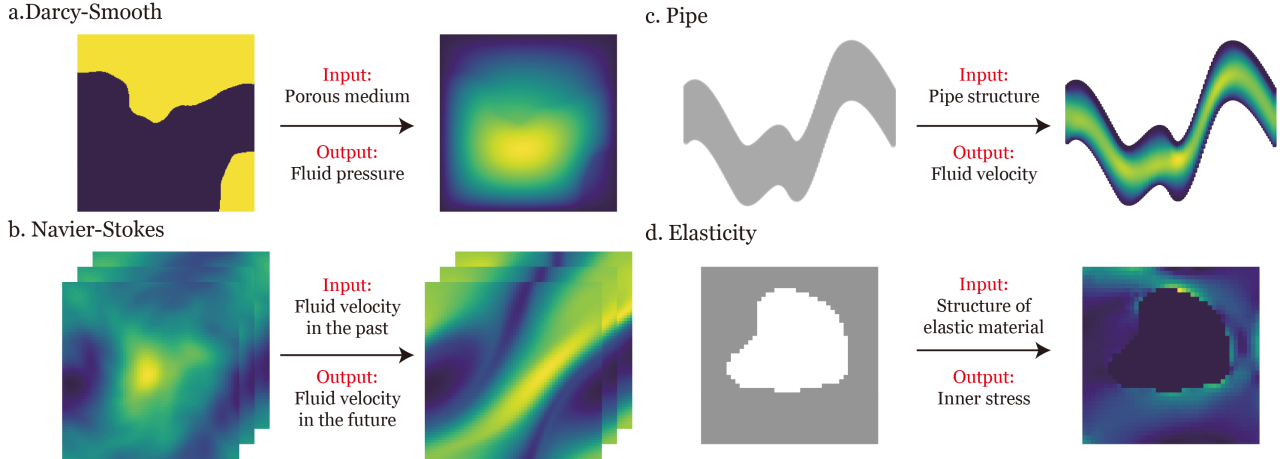


Figure 3. Examples of prediction tasks with dynamic spaces governed by PDEs. Datasets are named according to their underlying PDEs, including Darcy-Smooth, Navier-Stokes, Pipe, and Elasticity datasets. Networks should predict the states according to coefficients, previous solutions, and structures by approximating mappings between input and output in coordinate spaces. All the tasks are covered in our experiments.

Table 1. Experiment results on Multiscale Elliptic equations with various resolutions.  $\rightarrow$  denotes the resolution mapping between input and output, which are both rectangular. For example,  $256 \rightarrow 256$  denotes the input coefficient spaces are  $256 \times 256$  and the output solution spaces are  $256 \times 256$ . Performance is measured with mean squared error (MSE with  $\times 10^{-2}$ ). The number of parameters and time per epoch are measured for a batch size of 10. For clarity, the best result is in **bold** and the second best is underlined.

METHODS	PARAMETERS ( $\times 10^6$ )	TIME PER EPOCH (s)	TRIGONOMETRIC		DARCY ROUGH	
			256 $\rightarrow$ 256	512 $\rightarrow$ 512	128 $\rightarrow$ 128	256 $\rightarrow$ 256
FNO	2.42	7.42	1.936	1.932	2.160	2.098
WMT	10.32	20.03	1.043	1.087	1.573	1.621
U-NO	16.39	15.42	1.256	1.245	1.368	1.332
GT	3.27	36.32	1.143	1.264	2.231	2.423
F-FNO	4.87	10.42	1.429	1.424	1.435	1.513
HANO	15.84	29.13	<u>0.893</u>	<u>0.948</u>	<b>0.972</b>	1.241
DCNO	2.27	11.73	1.056	1.209	<u>1.176</u>	<u>0.948</u>
OURS	5.56	13.81	<b>0.778</b>	<b>0.863</b>	1.282	<b>0.919</b>

to correspondingly smooth solutions. We follow the setting in HANO [30] and DCNO [1] to modify the coefficients to two-phase rough ones (**Darcy-Rough**) or high-contrast trigonometric coefficients (**Trigonometric**). For example, in trigonometric setting, the coefficients are defined by  $a(x) = \prod_{k=1}^6 (1 + \frac{1}{2} \cos(a_k \pi (x_1 + x_2))) (1 + \frac{1}{2} \sin(a_k \pi (x_2 - 3x_1)))$ , where  $a_k$  is uniformly distributed between  $2^{k-1}$  and  $1.5 \times 2^{k-1}$  and the forcing term is fixed as  $f(x) \equiv 1$ . The original experiments of multiscale PDEs using coefficients with resolution  $1023 \times 1023$  to approximate the solution with resolution  $256 \times 256$  or  $512 \times 512$  in the trigonometric setting, which reduce the difficulties as larger inputs might contain more specific information. To enhance the difficulty, we modify the resolution of coefficients to the same as that of the output solution.

The experiment results are presented in Tab. 1, our model achieves the lowest error compared to other operator base-

lines in most situations, especially in the elliptic equations with trigonometric coefficients. Our results indicate that cascade architecture models, such as FNO and DCNO, perform suboptimally in this setting, while hierarchical structures, such as U-NO and HANO, perform relatively better. However, the amount of parameters and computations required by HANO and UNO are considerable, our model reduces the parameter quantity by using large kernel attention and convolutions and reaches better prediction performances. In order to better show the improvement of our model in solving multiscale PDEs, we visualize the prediction solution and error in Fig. 4.

## 4.2. Navier-Stokes Equation

We further consider fluid space governed by the 2D Navier-Stokes equation, in which the vorticity forms on the two-dimensional torus  $\mathbb{T}^2$ . Navier-Stokes equation is a standard

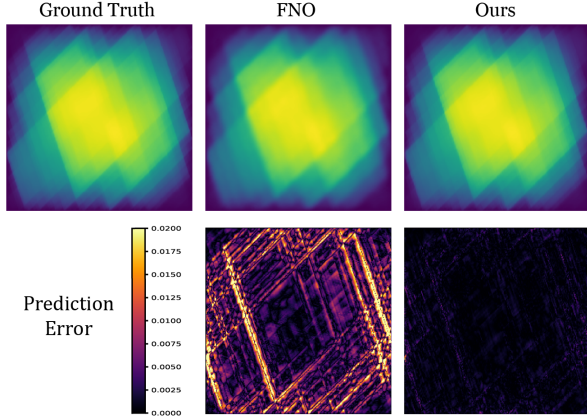


Figure 4. Showcase of Trigonometric multiscale PDEs. For clearness, we also plot the prediction error by the absolute error as  $|u - \hat{u}|$ .

benchmark proposed in FNO [26]. Details of the equation are in the Appendix. The vorticity is denoted as  $\omega(x, t)$ , where  $x \in \mathbb{T}^2$  and  $t \in [0, T]$  represent spatial domain and time interval respectively.

Specifically, the operator predicts the vorticity after  $T_0$  by the input vorticity before  $T_0$ , values of  $T_0$  and  $T$  vary according to the dataset. Our experiments consider viscosities with  $\nu \in \{10^{-3}, 10^{-4}, 10^{-5}, 10^{-6}\}$ , with smaller viscosities denoting more chaotic flow and are much harder to predict. To ensure fair comparisons, the ‘rollout’ strategy is employed to predict vorticity at each time step in a recursive manner. The final operator could be regarded as approximated by various neural operators.

Table 2. Experiments on various Navier-Stokes equations. Performances are measured with MSE ( $\times 10^{-2}$ ).  $N$  denotes the number of training samples. The resolutions are fixed at  $64 \times 64$  for both training and testing. Also, the best result is in **bold** and the second best is underlined.

METHODS	$\nu = 10^{-3}$	$\nu = 10^{-4}$	$\nu = 10^{-5}$	$\nu = 10^{-6}$
	$T_0 = 10s$ $T = 50s$ $N = 1000$	$T_0 = 10s$ $T = 30s$ $N = 10000$	$T_0 = 10s$ $T = 20s$ $N = 1000$	$T_0 = 6s$ $T = 15s$ $N = 5000$
FNO	1.28	8.34	19.82	5.28
WMT	1.01	11.35	15.41	4.95
U-NO	0.89	<b>5.72</b>	17.53	4.58
GT	1.12	-	26.84	-
F-FNO	0.92	6.02	17.98	4.32
HANO	0.98	6.18	18.47	<u>4.10</u>
LSM	<u>0.82</u>	6.12	<u>15.35</u>	4.53
OURS	<b>0.78</b>	<u>5.98</u>	<b>15.30</b>	<b>3.98</b>

Tab. 2 summarizes experimental results on Navier-Stokes equations with various coefficients. Our model performs better in almost all settings, especially in the dataset with small viscosities. As flows with smaller viscosities are

more chaotic, learning high-frequency features may help capture detailed flow changes.

### 4.3. Other physical scenarios

Table 3. Experiments on Elasticity, Darcy-Smooth, and Pipe physical datasets, all of which are generated from corresponding PDEs. Performances are measured with MSE ( $\times 10^{-2}$ ). Also, the best result is in **bold** and the second best is underlined.

METHODS	ELASTICITY	DARCY-SMOOTH	PIPE
FNO	5.08	1.08	0.67
WMT	5.20	0.82	0.77
U-NO	4.69	1.13	1.00
SNO	9.87	4.95	2.94
GT	16.81	1.70	0.98
HANO	4.72	0.79	0.59
F-FNO	4.75	0.77	0.70
LSM	<u>4.08</u>	<u>0.65</u>	<b>0.50</b>
OURS	<b>4.06</b>	<b>0.59</b>	<u>0.53</u>

We further evaluate our method on Pipe, Elasticity, and Darcy-Smooth datasets. The Pipe dataset focuses on predicting the incompressible flow through a pipe. The input is the structure of the pipe, while the output is the horizontal fluid velocity within the pipe. The Elasticity dataset is designed to predict the internal stress within an incompressible material containing an arbitrary void at its center and an external tensile force is exerted on the material. Originally, the Elasticity data are presented by the point clouds, we follow [46] to modify the data into regular grids. The input consists of the material’s structural characteristics, while the output represents the internal stress. The Darcy-Smooth dataset describes the flow of fluid through a porous medium. Compared to the multiscale PDE dataset presented in Sec. 4.1, the coefficients in the Darcy-Smooth dataset are much simpler. We evaluate our model on these datasets to demonstrate the effect of our model in solving general PDE problems. Our experimental results demonstrate that our model outperforms others in 2 out of 3 datasets. LSM [46], the previous state-of-the-art approach, utilizes a combination of self-attention and latent spectral decomposition to solve PDEs within the latent domain. Despite this, it is important to note that LSM is not an operator and it requires more computational resources since it relies on patchified multiscale architecture and self-attention mechanism. In contrast, our model is more concise and does not require a lot of hyperparameters. Other methods do not perform well in these three datasets.

### 4.4. Inverse Problems Solving

In various scientific disciplines such as geological sciences and mathematical derivation, inverse problems are of significant importance. Nonetheless, these problems frequently

demonstrate reduced stability compared to their associated forward problems, even when advanced regularization techniques are employed.

Table 4. Experiments on inverse coefficient identification tasks. In this experiment, the input solution space and output coefficient space are both  $256 \times 256$ . Performances are measured with MSE. Performances are measured with MSE ( $\times 10^{-2}$ ). Also, the best result is in **bold** and the second best is underlined.

METHODS	TRIGONOMETRIC			DARCY ROUGH		
	$\epsilon = 0$	$\epsilon = 0.01$	$\epsilon = 0.1$	$\epsilon = 0$	$\epsilon = 0.01$	$\epsilon = 0.1$
FNO	44.74	46.34	48.43	28.41	28.98	30.65
WMT	11.14	<u>12.43</u>	20.43	12.32	17.54	28.43
U-NO	12.97	18.54	25.87	15.64	20.54	25.34
GT	27.87	30.98	43.54	23.12	28.87	35.43
F-FNO	21.46	26.98	36.34	18.73	25.23	37.54
HANO	9.87	13.67	<u>20.98</u>	8.45	<u>10.43</u>	<u>20.43</u>
DCNO	<u>8.87</u>	17.64	34.76	<b>6.32</b>	11.83	23.54
OURS	<b>8.55</b>	<b>10.48</b>	<b>19.64</b>	<u>8.02</u>	<b>9.91</b>	<b>18.77</b>

Following [1], we evaluate our method for inverse identification problems on multiscale elliptic PDEs. In this experiment, we aim to learn an inverse operator, which maps the solution function space to the corresponding coefficient space  $\hat{u} = u + \epsilon N(u) \mapsto a$ . Here,  $\epsilon$  indicates the extent of Gaussian noise introduced into the training and evaluation data. The noise term  $N(u)$  accounts for the sampling distribution and data-related noise.

The experiments about inverse coefficients inference problems on the multiscale elliptic PDEs dataset are presented in Tab. 4. In our experiments, we modify the input and output resolutions to both  $256 \times 256$  in the Darcy Rough and Trigonometric elliptic equations. Since the coefficient function space changes faster than the solution space, this task is more challenging than the forward-solving problem.

The result shows that our model performs well in the inverse coefficient identification problem, which illustrates our model’s ability to successfully address the challenges posed by this ill-posed inverse problem with data. Methods such as FNO and F-FNO that learn kernel functions directly in the low-frequency domain have trouble recovering targets with high-frequency components. Furthermore, we find that methods with hierarchical architectures, like HANO and U-NO, are relatively robust in this scenario.

#### 4.5. Ablation study

To verify the effectiveness of each component in our model, we perform ablation studies in various settings, including removing components (w/o), replacing them with other components (rep), and adding some other components (add).

- In *w/o* part, we consider removing large kernel attention component (w/o LKA) or even the Fourier layer (w/o

Table 5. Ablation studies on our proposed model, including *removing components (w/o)*, *replacing them with other components (rep)*, and *adding some other components (add)*. Performances are measured with MSE ( $\times 10^{-2}$ ) and the best result is in **bold**.

DESIGNS		MSE		
		TRIGONO	DARCY-ROUGH	NAVIER-STOKES
W/O	LKA	0.981	1.103	18.23
	FNO	1.283	1.295	23.16
REP	CONV→RES	1.185	1.198	16.21
	CONV→FC	1.194	1.212	15.97
	LKA→D-CONV	0.884	0.927	16.47
	LKA→MLP	0.973	1.065	15.93
ADD	HIER	0.801	<b>0.912</b>	15.41
<b>OURS</b>		<b>0.778</b>	0.919	<b>15.30</b>

FNO).

- In *rep* part, we consider replacing the convolutional-residual layer and large kernel attention to other components and keep the number of parameters almost unchanged. For convolutional-residual layers, we replace them with simple residual layers (rep Conv→Res) or fully connected layers (rep Conv→Fc). For large kernel attention, we replace them with dilation convolution (rep LKA→d-Conv) or multi-layer perceptrons (rep LKA→MLP).
- In *add* part, we add more hierarchical layers (add Hier).

It is discovered that all components of our model are essential for solving multiscale PDEs after removing experiments. Without LKA and Fourier layer, model performance on all benchmarks will drop seriously, especially in multiscale PDEs tasks. Similar results could be found in replacing experiments, the convolutional-residual Fourier layer and LKA can fit the multiscale PDEs benchmarks well. Besides, in regular PDEs, MLP could achieve similar effects with LKA and dilation convolution, suggesting that previous methods can work well in PDEs where the coefficients do not change rapidly. Additionally, adding a hierarchical layer may improve the performance of the model sometimes, but this will add a significant amount of computation. To balance the efficiency and effectiveness we keep the number of layers of our model. Last but not least, we found our model generally performs better than methods with cascade architecture, such as FNO and F-FNO, indicating the importance of solving multiscale PDEs in a hierarchical way.

## 5. Conclusion

In this paper, we introduce a hierarchical Fourier neural operator that combines convolutional-residual Fourier layers and large kernel attentions for predicting dynamic spaces governed by multiscale PDEs. Our model utilizes Fourier



layers to learn low-frequency features, with convolutional-residual layer and large kernel attention to capture high-frequency local details. Benefits from the above components, our model could capture both local and global information and achieve superior performances in many PDE benchmarks. In the future, we wish to explore a foundation model for solving complex dynamics.

## References

- [1] Anonymous. Dilated convolution neural operator for multiscale partial differential equations. In *Submitted to The Twelfth International Conference on Learning Representations*, 2023. under review. [2](#), [4](#), [5](#), [6](#), [8](#)
- [2] Johannes Brandstetter, Rianne van den Berg, Max Welling, and Jayesh K Gupta. Clifford neural layers for pde modeling. *arXiv preprint arXiv:2209.04934*, 2022. [1](#)
- [3] Shuhao Cao. Choose a transformer: Fourier or galerkin. *Advances in neural information processing systems*, 34:24924–24940, 2021. [1](#), [2](#), [5](#)
- [4] Ricky TQ Chen, Yulia Rubanova, Jesse Bettencourt, and David K Duvenaud. Neural ordinary differential equations. *Advances in neural information processing systems*, 31, 2018. [1](#)
- [5] Salvatore Cuomo, Vincenzo Schiano Di Cola, Fabio Giampaolo, Gianluigi Rozza, Maziar Raissi, and Francesco Piccialli. Scientific machine learning through physics-informed neural networks: Where we are and what’s next. *Journal of Scientific Computing*, 92(3):88, 2022. [2](#)
- [6] Jifeng Dai, Haozhi Qi, Yuwen Xiong, Yi Li, Guodong Zhang, Han Hu, and Yichen Wei. Deformable convolutional networks. In *Proceedings of the IEEE international conference on computer vision*, pages 764–773, 2017. [3](#)
- [7] Jacob Devlin, Ming-Wei Chang, Kenton Lee, and Kristina Toutanova. Bert: Pre-training of deep bidirectional transformers for language understanding. *arXiv preprint arXiv:1810.04805*, 2018. [1](#)
- [8] Linhao Dong, Shuang Xu, and Bo Xu. Speech-transformer: a no-recurrence sequence-to-sequence model for speech recognition. In *2018 IEEE international conference on acoustics, speech and signal processing (ICASSP)*, pages 5884–5888. IEEE, 2018. [1](#)
- [9] Alex Furman. Modeling coupled surface–subsurface flow processes: a review. *Vadose Zone Journal*, 7(2):741–756, 2008. [2](#)
- [10] Zhengyang Geng, Meng-Hao Guo, Hongxu Chen, Xia Li, Ke Wei, and Zhouchen Lin. Is attention better than matrix decomposition? *arXiv preprint arXiv:2109.04553*, 2021. [3](#), [5](#)
- [11] Vignesh Gopakumar, Stanislas Pamela, Lorenzo Zanisi, Zongyi Li, Anima Anandkumar, and MAST Team. Fourier neural operator for plasma modelling. *arXiv preprint arXiv:2302.06542*, 2023. [2](#)
- [12] John Guibas, Morteza Mardani, Zongyi Li, Andrew Tao, Anima Anandkumar, and Bryan Catanzaro. Adaptive fourier neural operators: Efficient token mixers for transformers. *arXiv preprint arXiv:2111.13587*, 2021. [3](#)
- [13] Anmol Gulati, James Qin, Chung-Cheng Chiu, Niki Parmar, Yu Zhang, Jiahui Yu, Wei Han, Shibo Wang, Zhengdong Zhang, Yonghui Wu, et al. Conformer: Convolution-augmented transformer for speech recognition. *arXiv preprint arXiv:2005.08100*, 2020. [1](#)
- [14] Meng-Hao Guo, Tian-Xing Xu, Jiang-Jiang Liu, Zheng-Ning Liu, Peng-Tao Jiang, Tai-Jiang Mu, Song-Hai Zhang, Ralph R Martin, Ming-Ming Cheng, and Shi-Min Hu. Attention mechanisms in computer vision: A survey. *Computational visual media*, 8(3):331–368, 2022. [3](#)
- [15] Meng-Hao Guo, Cheng-Ze Lu, Zheng-Ning Liu, Ming-Ming Cheng, and Shi-Min Hu. Visual attention network. *Computational Visual Media*, 9(4):733–752, 2023. [3](#), [5](#)
- [16] Gaurav Gupta, Xiongye Xiao, and Paul Bogdan. Multiwavelet-based operator learning for differential equations. *Advances in neural information processing systems*, 34:24048–24062, 2021. [5](#)
- [17] Danijar Hafner, Timothy Lillicrap, Jimmy Ba, and Mohammad Norouzi. Dream to control: Learning behaviors by latent imagination. *arXiv preprint arXiv:1912.01603*, 2019. [1](#)
- [18] Zhongkai Hao, Songming Liu, Yichi Zhang, Chengyang Ying, Yao Feng, Hang Su, and Jun Zhu. Physics-informed machine learning: A survey on problems, methods and applications. *arXiv preprint arXiv:2211.08064*, 2022. [1](#), [2](#)
- [19] Zhongkai Hao, Zhengyi Wang, Hang Su, Chengyang Ying, Yinpeng Dong, Songming Liu, Ze Cheng, Jian Song, and Jun Zhu. Gnot: A general neural operator transformer for operator learning. In *International Conference on Machine Learning*, pages 12556–12569. PMLR, 2023. [1](#)
- [20] Kaiming He, Xiangyu Zhang, Shaoqing Ren, and Jian Sun. Deep residual learning for image recognition. In *Proceedings of the IEEE conference on computer vision and pattern recognition*, pages 770–778, 2016. [1](#)
- [21] Jacob Helwig, Xuan Zhang, Cong Fu, Jerry Kurtin, Stephan Wojtowytsch, and Shuiwang Ji. Group equivariant fourier neural operators for partial differential equations. *arXiv preprint arXiv:2306.05697*, 2023. [3](#)
- [22] Han Hu, Jiayuan Gu, Zheng Zhang, Jifeng Dai, and Yichen Wei. Relation networks for object detection. In *Proceedings of the IEEE conference on computer vision and pattern recognition*, pages 3588–3597, 2018. [3](#)
- [23] Jie Hu, Li Shen, and Gang Sun. Squeeze-and-excitation networks. In *Proceedings of the IEEE conference on computer vision and pattern recognition*, pages 7132–7141, 2018. [3](#)
- [24] Peter S Huyakorn. *Computational methods in subsurface flow*. academic press, 2012. [2](#)
- [25] George Em Karniadakis, Ioannis G Kevrekidis, Lu Lu, Paris Perdikaris, Sifan Wang, and Liu Yang. Physics-informed machine learning. *Nature Reviews Physics*, 3(6):422–440, 2021. [1](#), [2](#), [5](#)
- [26] Zongyi Li, Nikola Kovachki, Kamyar Azizzadenesheli, Burigede Liu, Kaushik Bhattacharya, Andrew Stuart, and Anima Anandkumar. Fourier neural operator for parametric partial differential equations. *arXiv preprint arXiv:2010.08895*, 2020. [2](#), [3](#), [5](#), [7](#)
- [27] Zongyi Li, Daniel Zhengyu Huang, Burigede Liu, and Anima Anandkumar. Fourier neural operator with learned de-

- formations for pdes on general geometries. *arXiv preprint arXiv:2207.05209*, 2022. [2](#), [3](#)
- [28] Zijie Li, Kazem Meidani, and Amir Barati Farimani. Transformer for partial differential equations’ operator learning. *arXiv preprint arXiv:2205.13671*, 2022. [1](#)
- [29] Songming Liu, Zhongkai Hao, Chengyang Ying, Hang Su, Ze Cheng, and Jun Zhu. Nuno: A general framework for learning parametric pdes with non-uniform data. *arXiv preprint arXiv:2305.18694*, 2023. [1](#)
- [30] Xinliang Liu, Bo Xu, and Lei Zhang. Ht-net: Hierarchical transformer based operator learning model for multiscale pdes. *arXiv preprint arXiv:2210.10890*, 2022. [2](#), [3](#), [4](#), [5](#), [6](#)
- [31] Zichao Long, Yiping Lu, Xianzhong Ma, and Bin Dong. Pde-net: Learning pdes from data. In *International conference on machine learning*, pages 3208–3216. PMLR, 2018. [2](#)
- [32] Lu Lu, Pengzhan Jin, and George Em Karniadakis. Deeponet: Learning nonlinear operators for identifying differential equations based on the universal approximation theorem of operators. *arXiv preprint arXiv:1910.03193*, 2019. [2](#)
- [33] Xuhui Meng, Zhen Li, Dongkun Zhang, and George Em Karniadakis. Ppinn: Parareal physics-informed neural network for time-dependent pdes. *Computer Methods in Applied Mechanics and Engineering*, 370:113250, 2020. [2](#)
- [34] J Merodio and RW Ogden. Instabilities and loss of ellipticity in fiber-reinforced compressible non-linearly elastic solids under plane deformation. *International Journal of Solids and Structures*, 40(18):4707–4727, 2003. [2](#)
- [35] Oded Ovadia, Adar Kahana, Panos Stinis, Eli Turkel, and George Em Karniadakis. Vito: Vision transformer-operator. *arXiv preprint arXiv:2303.08891*, 2023. [3](#)
- [36] Oded Ovadia, Eli Turkel, Adar Kahana, and George Em Karniadakis. Ditto: Diffusion-inspired temporal transformer operator. *arXiv preprint arXiv:2307.09072*, 2023. [3](#)
- [37] Jaideep Pathak, Shashank Subramanian, Peter Harrington, Sanjeev Raja, Ashesh Chattopadhyay, Morteza Mardani, Thorsten Kurth, David Hall, Zongyi Li, Kamyar Azizzadenesheli, et al. Fourcastnet: A global data-driven high-resolution weather model using adaptive fourier neural operators. *arXiv preprint arXiv:2202.11214*, 2022. [2](#)
- [38] Alfio Quarteroni and Alessandro Veneziani. Analysis of a geometrical multiscale model based on the coupling of ode and pde for blood flow simulations. *Multiscale Modeling & Simulation*, 1(2):173–195, 2003. [2](#)
- [39] Md Ashiqur Rahman, Zachary E Ross, and Kamyar Azizzadenesheli. U-no: U-shaped neural operators. *arXiv preprint arXiv:2204.11127*, 2022. [5](#)
- [40] Yongming Rao, Wenliang Zhao, Zheng Zhu, Jiwen Lu, and Jie Zhou. Global filter networks for image classification. *Advances in neural information processing systems*, 34:980–993, 2021. [3](#)
- [41] RSI Rivlin. Large elastic deformations of isotropic materials. i. fundamental concepts. *Philosophical Transactions of the Royal Society of London. Series A, Mathematical and Physical Sciences*, 240(822):459–490, 1948. [2](#)
- [42] Arnold Sommerfeld. *Partial differential equations in physics*. Academic press, 1949. [1](#)
- [43] Joakim Sundnes, Glenn Terje Lines, and Aslak Tveito. An operator splitting method for solving the bidomain equations coupled to a volume conductor model for the torso. *Mathematical biosciences*, 194(2):233–248, 2005. [2](#)
- [44] Alasdair Tran, Alexander Mathews, Lexing Xie, and Cheng Soon Ong. Factorized fourier neural operators. *arXiv preprint arXiv:2111.13802*, 2021. [3](#), [5](#)
- [45] Sanghyun Woo, Jongchan Park, Joon-Young Lee, and In So Kweon. Cbam: Convolutional block attention module. In *Proceedings of the European conference on computer vision (ECCV)*, pages 3–19, 2018. [3](#)
- [46] Haixu Wu, Tengge Hu, Huakun Luo, Jianmin Wang, and Mingsheng Long. Solving high-dimensional pdes with latent spectral models. *arXiv preprint arXiv:2301.12664*, 2023. [5](#), [7](#)
- [47] Yuhui Yuan, Xilin Chen, and Jingdong Wang. Object-contextual representations for semantic segmentation. In *Computer Vision–ECCV 2020: 16th European Conference, Glasgow, UK, August 23–28, 2020, Proceedings, Part VI 16*, pages 173–190. Springer, 2020. [3](#), [5](#)
- [48] Tielin Zhang, Xiang Cheng, Shuncheng Jia, Chengyu T Li, Mu-ming Poo, and Bo Xu. A brain-inspired algorithm that mitigates catastrophic forgetting of artificial and spiking neural networks with low computational cost. *Science Advances*, 9(34):eadi2947, 2023. [1](#)
- [49] Xuanle Zhao, Duzhen Zhang, Liyuan Han, Tielin Zhang, and Bo Xu. Ode-based recurrent model-free reinforcement learning for pomdps. *arXiv preprint arXiv:2309.14078*, 2023. [1](#)
- [50] Peng Zhou, Wei Shi, Jun Tian, Zhenyu Qi, Bingchen Li, Hongwei Hao, and Bo Xu. Attention-based bidirectional long short-term memory networks for relation classification. In *Proceedings of the 54th annual meeting of the association for computational linguistics (volume 2: Short papers)*, pages 207–212, 2016. [1](#)
- [51] Tian Zhou, Ziqing Ma, Qingsong Wen, Xue Wang, Liang Sun, and Rong Jin. Fedformer: Frequency enhanced decomposed transformer for long-term series forecasting. In *International Conference on Machine Learning*, pages 27268–27286. PMLR, 2022. [3](#)